

Noble-metal adsorption on Si(111): Medium-energy ion-scattering results for the Ag ($\sqrt{3} \times \sqrt{3}$)R 30° reconstruction

M. Copel and R. M. Tromp

IBM Research Division, Thomas J. Watson Research Center, P.O. Box 218, Yorktown Heights, New York 10598

(Received 28 December 1988)

The geometric structure of the Si(111)-($\sqrt{3} \times \sqrt{3}$)R30° Ag surface has previously been studied by numerous surface-science techniques. Despite the abundance of data, no model for the surface has emerged as a clear favorite. Commonly proposed models feature honeycomb structures of either Ag or Si, with two or three Ag atoms per $\sqrt{3} \times \sqrt{3}$ unit cell. Results from medium-energy ion scattering conclusively show that each unit cell contains three Ag atoms. In addition, the surface is highly reconstructed, with atomic reordering of the Si atoms of similar magnitude to the clean (7×7) surface. Conventional models of the surface do not incorporate sufficient displacements of silicon atoms. Two new models are compatible with our results. One is a model constructed from silicon adatoms and vacancies. The other is a model based on x-ray scattering results, consisting of a sub-surface silver honeycomb-chained trimer.

Most metals interact strongly with silicon, forming silicide layers with a complex morphology that does not lend itself to detailed structural analysis of the Si-silicide interface. An exceptional case is the Ag-Si interface, where there is no silicide formation. Highly regular surfaces with near monolayer Ag coverage can be prepared exhibiting excellent long-range ($\sqrt{3} \times \sqrt{3}$)R 30° order.¹⁻³ Given the small size of the unit cell, one would expect that determination of the $\sqrt{3} \times \sqrt{3}$ structure would be a relatively straightforward problem. However, studies with a multitude of probes¹⁻¹⁰ have failed to reach a consensus. There are conflicting results on both the silver coverage and the role of substrate reconstruction in the $\sqrt{3} \times \sqrt{3}$ surface. In the present study, we will show that the $\sqrt{3} \times \sqrt{3}$ surface undergoes a complex reconstruction, largely neglected by previous studies, which has hindered determination of the structure. The reconstruction is evident by the large backscattering yields measured with medium-energy ion scattering (MEIS). The atomic displacements of the silicon surface are comparable in magnitude to those occurring in the (7×7) reconstruction seen on clean Si(111).¹¹

What features must be included in a successful model of the Si(111)-($\sqrt{3} \times \sqrt{3}$)R 30° surface? From scanning-tunneling-microscopy (STM) studies, we require that the outermost layer of atoms be in a honeycomb (HC) pattern.^{1,2} In addition, STM images showing adjacent regions of $\sqrt{3} \times \sqrt{3}$ and (7×7) have been used to show that the honeycomb layer is most likely above the threefold hollow site (H_3).³ Surface extended x-ray-absorption fine-structure spectroscopy (SEXAFS) results suggest that silver and silicon atoms are very nearly coplanar.⁶ In the present study, we will add the requirement that 1 monolayer (ML) of silicon must be laterally displaced from bulk sites, and 2 ML must be vertically displaced. The ion scattering results alone are sufficient to effectively eliminate the commonly proposed models of the $\sqrt{3} \times \sqrt{3}$ surface.

For a model to successfully describe the $\sqrt{3} \times \sqrt{3}$ surface, it must be compatible with the electronic structure of the $\sqrt{3} \times \sqrt{3}$ surface, which includes a surface-state gap at the Fermi energy.^{1,12,13} In order to form a gap by hybridization, the total number of valence electrons must be even. In each $\sqrt{3} \times \sqrt{3}$ unit cell, 3 electrons are supplied by the substrate p_z orbitals. To complement these, we need an odd number of Ag atoms. A silver honeycomb contains two Ag atoms per $\sqrt{3} \times \sqrt{3}$ unit cell, which is not compatible with a semiconducting surface. It is only with full monolayer coverage, i.e., three Ag atoms per $\sqrt{3} \times \sqrt{3}$ unit cell, that a band gap can form. This is substantiated by our coverage measurements. As an alternative to monolayer coverage, Kono *et al.*¹⁰ have proposed that the bulk donates an extra electron to the $\sqrt{3} \times \sqrt{3}$ surface, resulting in a charged surface with a band gap and $\frac{2}{3}$ monolayer coverage. Not only does this conflict with our coverage determination, but we will show below that the currently proposed silver-honeycomb model conflicts with our data.

EXPERIMENT

Samples were prepared and analyzed in an ultrahigh-vacuum system equipped with low-energy electron diffraction and Auger-electron spectroscopy. There was no chemical precleaning of substrates (Virginia Semiconductor, *n*-type As 5 mΩ cm). Prior to Ag deposition, a clean Si(111)-(7×7) surface was prepared by a standard procedure of degassing and light sputtering followed by oxide flash-off.¹¹ Ag was evaporated from a Tungsten filament while the sample was held at 500°C. A typical deposition time was 5 min, during which the chamber pressure remained in the 10⁻¹⁰-torr regime. The preparation method is the same as used in several STM studies which found large areas of well-ordered $\sqrt{3} \times \sqrt{3}$ domains.^{1,3}

Backscattered ions were energy analyzed with toroidal

electrostatic deflection plates and detected with channel plates and a position-sensitive detector. For a detailed review of the experimental technique, see Ref. 14. Due to scattering kinematics, protons backscattered from silicon and silver result in two well-resolved peaks at different energies. It is therefore possible to distinguish between the two.

Ag coverage was 0.85 ± 0.05 ML, as determined with the ion beam ($1 \text{ ML} = 7.83 \times 10^{14} \text{ atoms/cm}^2$). In previous experiments on the Si(111)-(1 \times 1)As surface, with a nominal coverage of 1 ML, the largest coverage obtained was 0.93 ML.^{15,16} Assuming that the deficit in coverage is a result of defects and/or steps, we would expect a larger unit cell, such as the $\sqrt{3} \times \sqrt{3}$, to be more sensitive to surface defects. Since the coverage is somewhat less than 1 ML, but significantly more than $\frac{2}{3}$ ML, we conclude that the nominal coverage is 1 ML, and each $\sqrt{3} \times \sqrt{3}$ unit cell contains three Ag atoms. In all experimental geometries examined, the Ag scattering yield was unaffected by either shadowing or blocking. From this, we can conclude that if the silver is subsurface, it is not located in a bulk symmetry site. Furthermore, the lack of any shadowing effects indicates that there is no epitaxial islanding of the Ag that would cause us to overestimate the coverage of the $\sqrt{3} \times \sqrt{3}$ phase.

Channeling experiments were performed using 100-keV protons aligned in four different experimental geometries. For the sake of brevity, we will only discuss two geometries, although our analysis of the entire data set resulted in the same conclusions. Backscatter yields from the silicon with the crystal aligned to an off-normal channeling direction are shown in Fig. 1. Yields for the $\sqrt{3} \times \sqrt{3}$ surface (circles) exceed simulations for a bulk-like termination (dotted curve) by nearly 1 atom/row. In this scattering geometry, shown at the top of Fig. 1, 2 ML is equivalent to 1 atom/row. For 100 keV protons channeling in the [00 $\bar{1}$] direction, a silicon atom must be $\geq 0.2 \text{ \AA}$ from a bulk site to no longer shadow the underlying substrate. The magnitude of the displacement is larger than expected for simple bond-length distortion on the surface, but is closer to that expected for a surface reconstruction. Indeed, yields from the $\sqrt{3} \times \sqrt{3}$ surface are virtually indistinguishable from yields from the clean (7 \times 7) reconstructed surface (squares).

Likewise, in a scattering geometry with a normally incident beam (Fig. 2), yields for the $\sqrt{3} \times \sqrt{3}$ surface (circles) closely resemble results for the (7 \times 7) surface (squares). Here, 1 ML of silicon must be displaced $\geq 0.1 \text{ \AA}$ from bulk sites to account for the extra backscatter yield. (In this geometry 3 ML=1 atom per row.) The high scattering yield at normal incidence must be due to lateral movement of silicon, eliminating vertical relaxations as the sole mechanism for displacement of silicon.

DISCUSSION

The high backscatter yield of the (7 \times 7) surface can be attributed to two features of the reconstructed unit cell.^{11,17} First, there is a stacking fault extending over half of the unit cell and, second, there are silicon adatoms tying up dangling bonds. The result is a surface with a

large number of atoms that no longer shadow the underlying silicon, giving yields that closely resemble experiment (Fig. 1, solid curve). As was the case for the (7 \times 7) dimer-adatom-stacking-fault (DAS) reconstruction, results for the $\sqrt{3} \times \sqrt{3}$ surface suggest some lateral movement of the silicon coupled to a larger vertical reconstruction. But the full range of structural components in the DAS model is not available for a $\sqrt{3} \times \sqrt{3}$ reconstruction; the unit cell is too small to accommodate a stacking fault unless it extends over the entire surface. Nonetheless, the ion scattering results indicate that an extensive reconstruction of the silicon lattice occurs, which may have structural components reminiscent of the (7 \times 7) surface.

Proposed models of the $\sqrt{3} \times \sqrt{3}$ surface can be divided into two categories: models with silver adsorbed outside of the silicon lattice, and models that embed the silver, or have it nearly coplanar with the outermost silicon layer. Models that do not embed the silver generally do not involve significant lattice distortion of the underlying silicon. Thus, our results would tend to favor models with embedded or coplanar silver, where larger atomic displacements are expected.

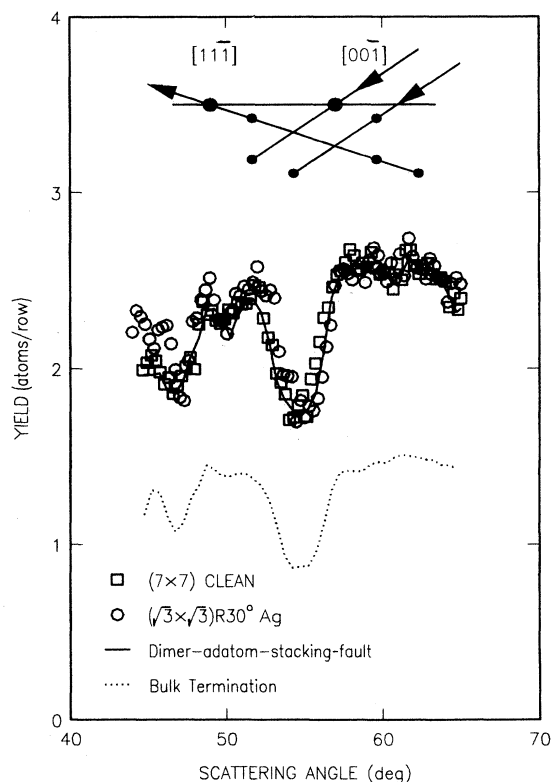


FIG. 1. Si backscattering yields from the Si(111)-(7 \times 7) surface (\square) and the Si(111)-($\sqrt{3} \times \sqrt{3}$)R30 $^\circ$ Ag surface (\circ). The curves are simulations for the dimer-adatom-stacking fault model of the (7 \times 7) reconstruction (solid curve), and for a bulk-like termination of the surface (dotted curve). The scattering geometry is indicated at the top of the figure.

We compare computer simulations of ion scattering yields with experimental results for off-normal the scattering geometry in Fig. 3. The simulation for a silver-honeycomb model (solid curve), greatly underestimates the experimental yields. In this model the silver is located outside of the surface, in the H_3 site. The atomic coordinates for the simulation were taken from self-consistent total-energy calculations based on minimization of Hellman-Feynman forces.¹⁸ Similar atomic coordinates may be derived from simple bond-length considerations. Since relatively small displacements of the silicon have been used (≈ 0.1 Å), the calculated yields are not very much greater than for a bulk termination.

An alternative to the silver-honeycomb model is the embedded-trimer (ET) model, drawn in top view in Fig. 4(a). The ET model consists of a full monolayer of Ag embedded between the first and second silicon layers, with trimerization of the silver. The outermost silicon layer contains vacancies above the centers of the trimers, causing a honeycomb arrangement as seen by STM.¹ The yields of the ET model are somewhat greater than for the HC model (Fig. 3), but still fall below experiment. Embedding the silver between the first and second silicon layers gives rise to significant lattice distortions, but the

displacements of the silicon must be vertical due to symmetry considerations. In the simulations of Fig. 3, the outermost silicon double layer has been expanded to a spacing of 1.5 Å, with the silver layer 0.3 Å beneath the surface. All of the lateral displacements are in the silver layer, which has been trimerized to give a silver-silver spacing of 2.8 Å. For the ET model there are two possible stacking sequences: The silver trimer can be in either a substitutional site (type *A*), with the Si outer layer in the H_3 site, or in a stacking order rotated 180° (type *B*) with the silicon outer layer in a bulk site. We show simulated yields from both sequences, and neither brings the model into agreement with data, nor does taking a linear superposition of the two types as suggested in Ref. 19.

We have optimized the ET model by distorting the type-*A* structure as far as possible (Fig. 3, dot-dashed curve). To do this, we have broken the symmetry of the model and allowed a 0.2-Å vertical buckling of the silicon extending to the second atomic plane. We have also included a 0.3-Å rotation of both the silver and the second silicon layer and a 0.3-Å lateral movement of the second silicon layer towards the first layer sites. The physical motivation for the buckling and the trimer rotation is to relieve compression of the Ag—Si bond. The effect on

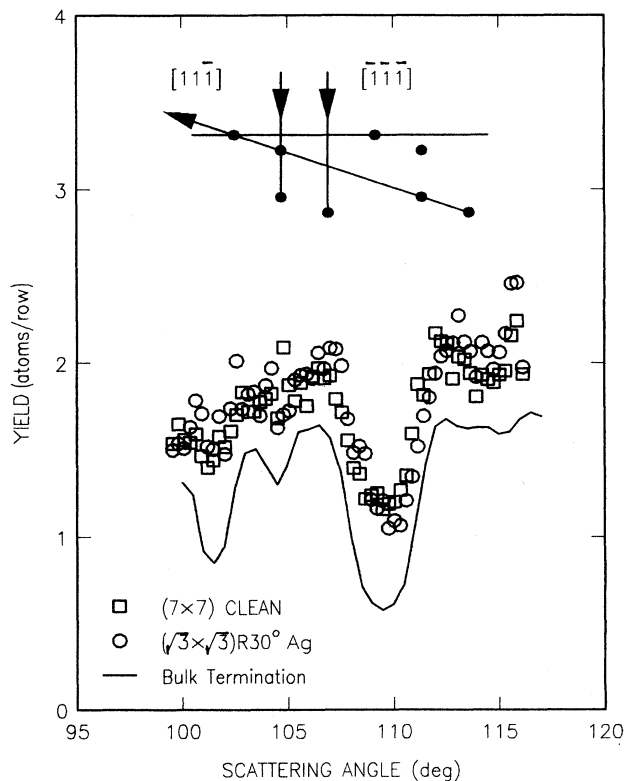


FIG. 2. Si backscattering yields for normal incidence on the Si(111)-(7 \times 7) surface (\square) and the Si(111)-($\sqrt{3}\times\sqrt{3}$)R30° Ag surface (\circ). The solid curve is a simulation for a bulklike termination of the surface. The scattering geometry is indicated at the top of the figure.

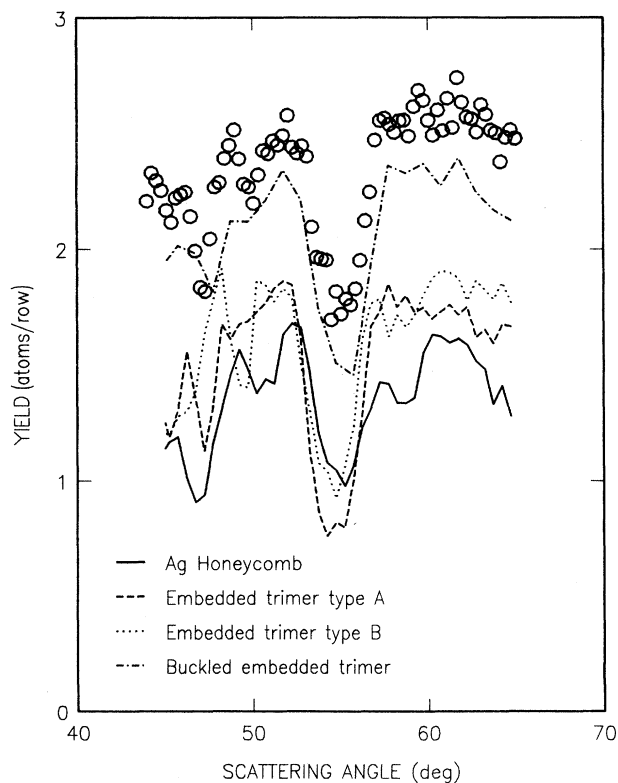


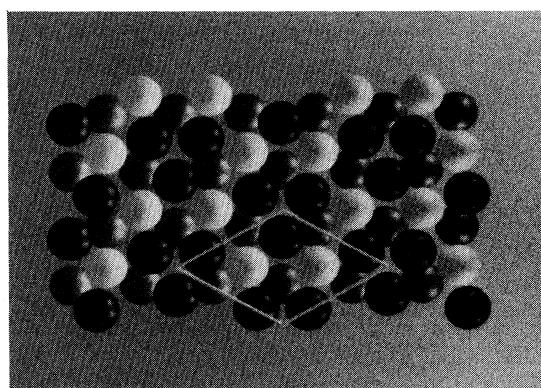
FIG. 3. Si backscattering yields from the Si(111)-($\sqrt{3}\times\sqrt{3}$)R30° Ag surface. The curves are simulations for the silver honeycomb model and various embedded trimer models of the reconstructed surface, as described in the text. The scattering geometry is the same as in Fig. 1.

our simulations is to raise the yields at glancing incidence without affecting the yields at normal incidence. We do not wish to emphasize the exact details of the buckled ET model, but we do wish to emphasize that a highly complex structure must be postulated in order to bring the ET model into agreement with experiment. Indeed, the buckled ET model involves greater lattice distortion than

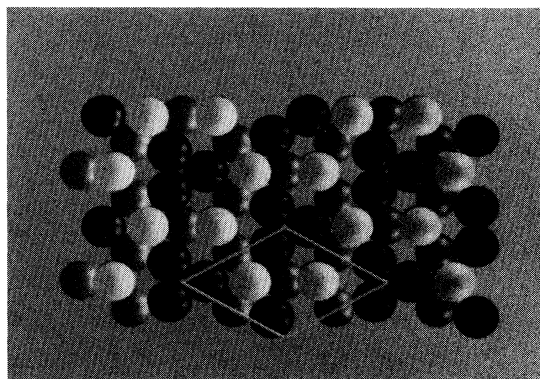
suggested by theory.¹⁸ In addition, the trimer rotation used in this model breaks the threefold symmetry of the surface, making this model unrealistic.

The data for the $\sqrt{3} \times \sqrt{3}$ surface include not only the silicon backscatter yields, but also the isotropic Ag backscatter yields (Fig. 5). The scattering geometry used was the same as in Fig. 1, with an off-normal angle of incidence, but data taken in normal incidence are nearly identical. A simulation for the HC model does indeed result in an isotropic yield, but in poor agreement with experiment (dashed curve). The discrepancy is an unavoidable feature of the HC model, since the coverage is only $\frac{2}{3}$ ML. The ET model also fails to describe our yields. For the type-*A* stacking (dashed curve), there is shadowing of the silver by the first silicon layer. For type-*B* stacking (dotted curve), there is blocking by the silicon. The shadowing and blocking of backscattering from Ag can only be eliminated by rotating the Ag trimer, so that it is no longer in the same lattice plane as the Si, as in the buckled ET model (dot-dashed curve).

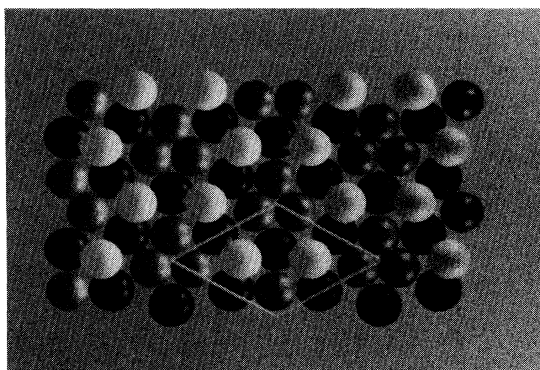
In light of the failure of the above models, it is appropriate to look for models featuring reconstruction of the silicon substrate itself. Two models show promising agreement with the MEIS results: the silicon adatom-vacancy (SAV) model and the silver honeycomb-chained



(a) Embedded Trimer Model



(b) Silicon Adatom-Vacancy Model



(c) Silver Honeycomb-Chained Trimer Model

FIG. 4. Models of the Si(111)-($\sqrt{3} \times \sqrt{3}$) $R30^\circ$ Ag surface. Top views include (a) the embedded trimer model, (b) the silicon adatom-vacancy model, and (c) the silver honeycomb-chained trimer model. Silver atoms are represented by the larger diameter spheres, and a $\sqrt{3} \times \sqrt{3}$ unit cell is indicated.

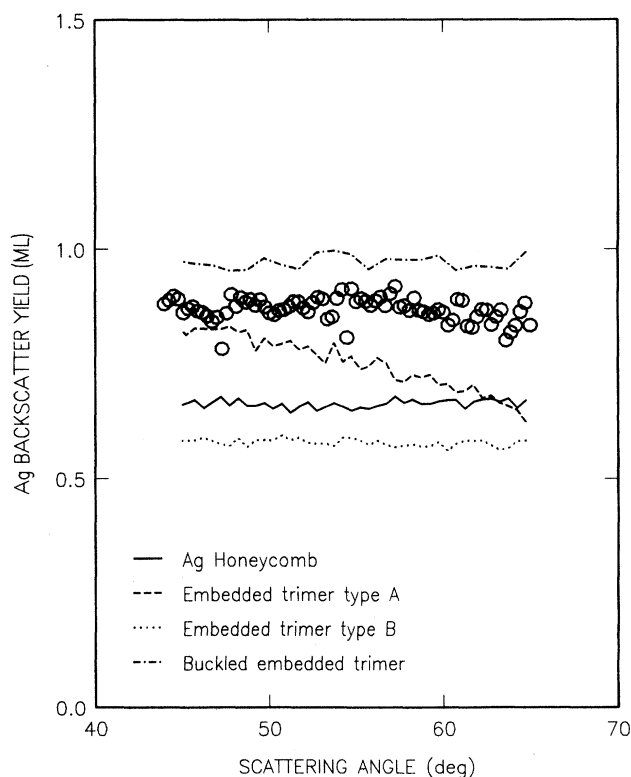


FIG. 5. Backscattering yields from Ag in the Si(111)-($\sqrt{3} \times \sqrt{3}$) $R30^\circ$ Ag surface. The curves are simulations for models of the reconstructed surface, as described in the text. The scattering geometry is the same as in Fig. 1.

TABLE I. Coordinates for the silicon adatom-vacancy model of the Si(111)-($\sqrt{3}\times\sqrt{3}$)R30° surface. X and Y coordinates are normalized to $\sqrt{3}\times\sqrt{3}$ unit-cell vectors. Z coordinates are in angstroms.

Layer	X	Y	Z	Atom
1	0.333	0.667	0.000	Si
1	0.667	0.333	-0.200	Si
2	0.238	0.118	0.000	Ag
2	0.882	0.118	0.000	Ag
2	0.882	0.762	0.000	Ag
3	0.500	0.000	1.727	Si
3	0.500	0.500	1.727	Si
3	0.000	0.500	1.727	Si
4	0.333	0.667	2.822	Si
4	0.667	0.333	3.024	Si

TABLE II. Coordinates for the silver honeycomb-chained trimer model of the Si(111)-($\sqrt{3}\times\sqrt{3}$)R30° surface. X and Y coordinates are normalized to $\sqrt{3}\times\sqrt{3}$ unit-cell vectors. Z coordinates are in angstroms.

Layer	X	Y	Z	Atom
1	0.333	0.667	0.000	Si
1	0.667	0.333	0.000	Si
2	0.426	0.000	1.724	Ag
2	0.575	0.575	1.724	Ag
2	0.000	0.426	1.724	Ag
3	0.000	0.805	2.487	Si
3	0.195	0.195	2.487	Si
3	0.805	0.000	2.487	Si

trimer (SHCT) model.²⁰ Both models include a full monolayer of subsurface silver. Also, both models feature the combination of silicon adatoms and large displacements of silicon from bulk sites. The models differ in both the adatom site, the silver coordination, and the structure of the second silicon layer. The SAV model [Fig. 4(b)] is composed of a layer of silicon adatoms nearly coplanar with a trimerized layer of silver. The outer-

most silicon double layer is severely distorted by both the adatoms and by vacancies in the inner half of the double layer. There is one vacancy per $\sqrt{3}\times\sqrt{3}$ unit cell, located in the center of trimers. Because of the vacancies, there is now more room to embed the silver trimers without unrealistic silver-silicon bond lengths. Note that the silver trimers are not in the same orientation as in the ET model, but are rotated by 30°. Because the vacancies allow room for a full 30° rotation, unlike the buckled ET model, the threefold symmetry of the surface is

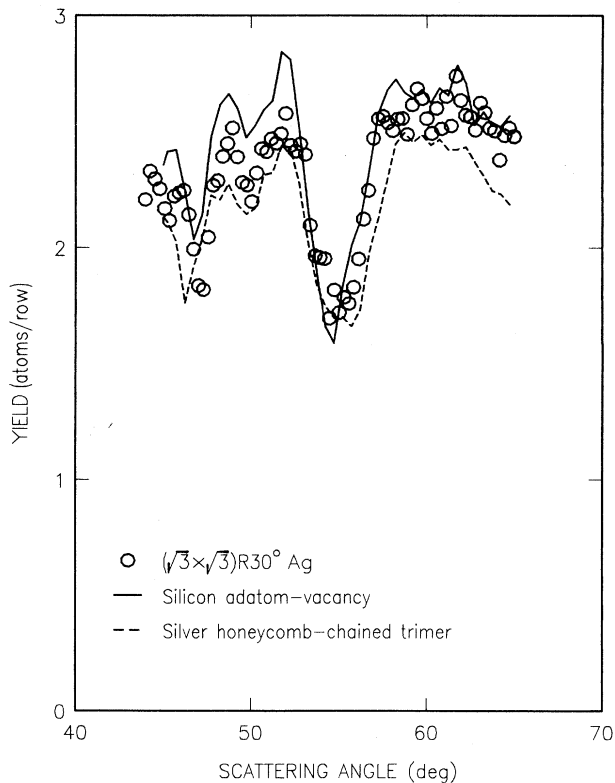


FIG. 6. Si backscattering yields from the Si(111)-($\sqrt{3}\times\sqrt{3}$)R30° Ag surface. The curves are simulations for the silicon adatom-vacancy (solid curve) and the silver honeycomb-chained trimer (dashed curve) models of the $\sqrt{3}\times\sqrt{3}$ surface. The scattering geometry is the same as in Fig. 1.

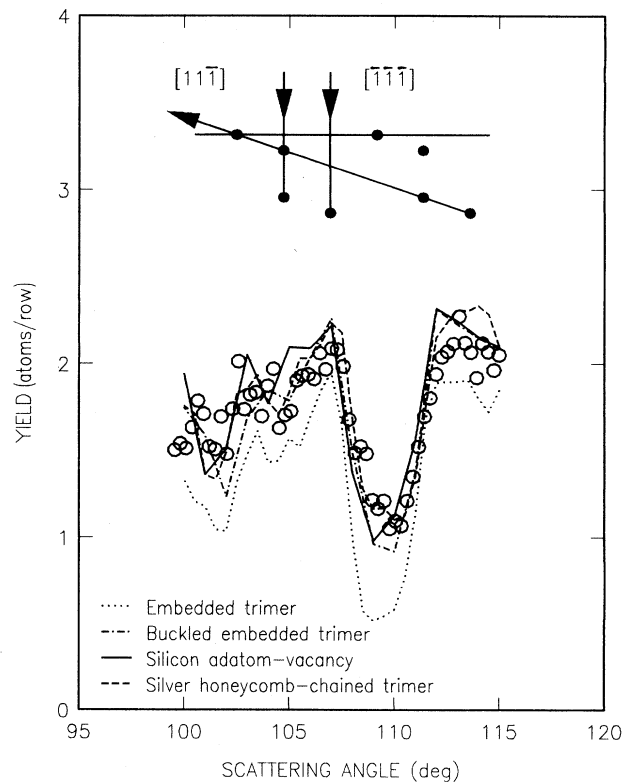


FIG. 7. Si backscattering yields for normal incidence on the Si(111)-($\sqrt{3}\times\sqrt{3}$)R30° Ag surface. The curves are simulations for models of the reconstructed surface, as described in the text. The scattering geometry is indicated at the top of the figure.

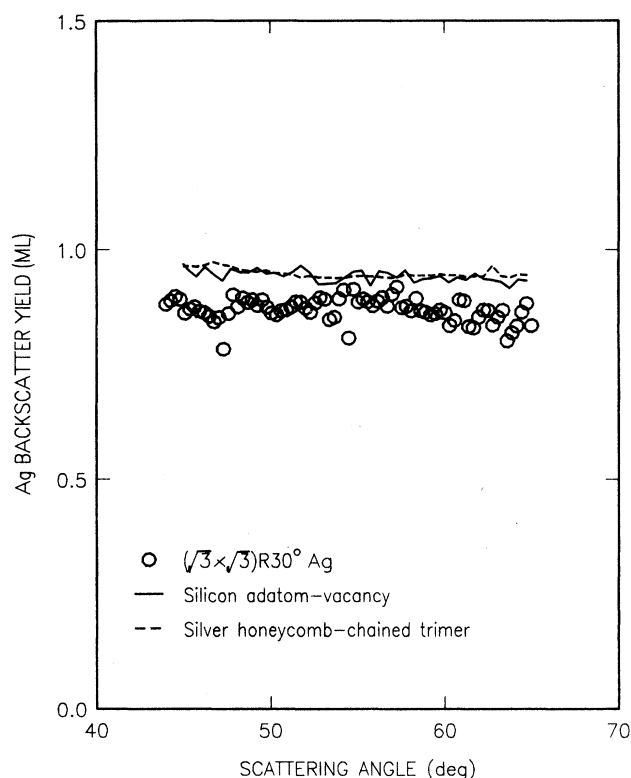


FIG. 8. Backscattering yields from Ag in the Si(111)- $(\sqrt{3}\times\sqrt{3})R30^\circ$ Ag surface. The curves are simulations for silicon adatom-vacancy (solid curve) and the silver honeycomb-chained trimer (dashed curve) models of the $\sqrt{3}\times\sqrt{3}$ surface. The scattering geometry is the same as in Fig. 1.

preserved. The rotation has the effect of inducing a $0.2\text{-}\text{\AA}$ buckling of the Si adatoms and the third layer atoms directly underneath the adatoms. Our results are relatively insensitive to the exact coordinates of the silver trimers, as long as they are located far from the silicon scattering planes, which is indeed the effect of the 30° ro-

tation. The atomic coordinates for the SAV model are listed in Table I. A chief advantage to the model is the reasonable nature of the structural components: adatoms are thought to be an integral part of silicon and germanium (111) surfaces.^{17,21} Furthermore, simulations show an excellent agreement with MEIS data (Fig. 6). A disadvantage to the SAV model is that somewhat extensive bond compression seems to be required for a good fit to MEIS data. The shortest Si—Si bond length is 2.22 \AA , compared to the bulk bond length of 2.35 \AA , and Ag—Si bond lengths are in the range of 2.5 \AA . The bond lengths are not, however, intrinsic to the SAV structure, but were treated as fitting parameters for modeling MEIS data. A more severe problem arises from the site of the outermost layer, located above the second-layer silicon (T_4). STM results suggest that the outermost layer is located in the H_3 site, conflicting with the SAV model.³

The SHCT model, based on x-ray scattering results, invokes several unusual features [Fig. 4(b)]. First, the silver monolayer does not trimerize, but moves radially outward, forming a honeycomb chain centered underneath the adatoms. A similar arrangement of silver atoms was proposed in an independent analysis of x-ray scattering results.²² The model proposed by Vlieg *et al.*²⁰ includes not only the silver coordination, but details of the silicon sites. There are two main features that deviate from the bulk structure: first, a honeycomb of silicon atoms outside of the silver layer, and second, a layer of silicon trimers centered within the honeycomb. Due to the unique bonding topology, the silicon trimers are located far from bulk sites and the backscatter yields are high enough to show good agreement with MEIS data (Fig. 6). The coordinates used in our simulations, taken from Vlieg *et al.* are listed in Table II. An advantage to this model is that the outermost atomic layer is located in the H_3 site, in agreement with STM results. Ag—Si bond lengths are about 2.6 \AA , which is not as compressed as in the SAV model, however the distance between trimerized Si atoms is 2.25 \AA , nearly as short as the smallest bond lengths in the SAV model.

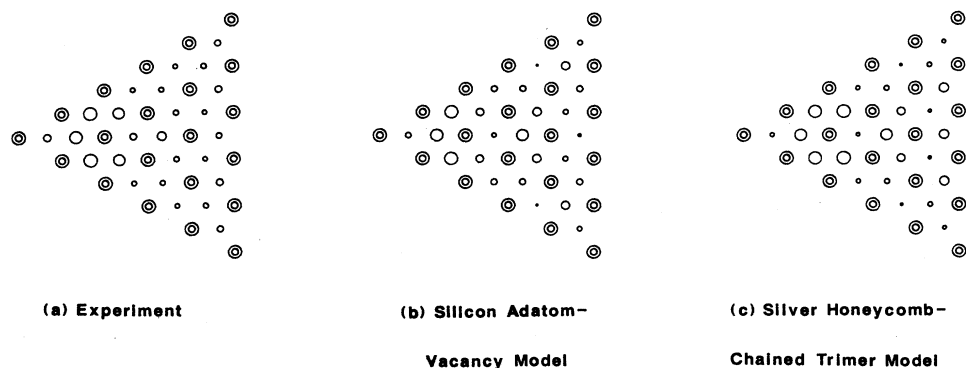


FIG. 9. X-ray diffraction patterns for the Si(111)- $(\sqrt{3}\times\sqrt{3})R30^\circ$ Ag surface. Only 60° of the pattern is shown, with the (0,0) spot at the far left. Integer-order spots are represented by two concentric circles, fractional-order beams are drawn with radii proportional to the square root of the intensity. (a) Experimental data, (b) silicon adatom-vacancy model, and (c) silver honeycomb-chained trimer model are shown.

Two further tests may be applied to the SAV and SHCT models. First, we can compare the models with the backscatter yields from a normal incidence experiment (Fig. 7). Both the SAV model (solid curve) and the SHCT model (dashed curve) fit the data quite well, especially when compared with the ET model (dotted curve). A second test is the absence of either blocking or shadowing of the Ag backscatter yield, shown in Fig. 8. Since the silver has been removed from the silicon scattering planes, isotropic backscattering is predicted for both models.

Since both the SAV and SHCT models demonstrate reasonable agreement with MEIS results, other evidence must be used to distinguish which model, if either, is the more realistic. A comparison of calculated x-ray diffraction patterns with the data from Ref. 20 is instructive (Fig. 9). The patterns were calculated using a two-dimensional kinematic approximation, including the individual atomic form factors and a single Debye-Waller factor for all of the atoms. Intensities were not calculated for integral-order spots, which are represented as having a uniform intensity. For simplicity, we show only one 60° sector of the diffraction pattern, eliminating the symmetrically equivalent sectors. The radius of each circle is proportional to the square root of the diffracted intensity. Visual inspection of the patterns show that both models resemble experiment, although no effort was made to optimize the Debye-Waller parameters. However, a quantitative comparison of χ^2 factors distinctly favors the SHCT model.

CONCLUSIONS

We have analyzed ion scattering results from the Si(111)-($\sqrt{3} \times \sqrt{3}$)R 30° Ag surface in detail. Both the extensive reconstruction of the surface and the silver coverage tend to argue against a silver honeycomb adsorbed outside of the surface. Furthermore, the isotropic backscattering from the silver eliminates the possibility of an embedded trimer model, at least as conventionally described. Experimental results can only be modeled by a complex reconstruction of the surface involving lateral displacements of 2 ML of silicon, vertical displacements of 1 ML of silicon, and full monolayer coverage of silver.

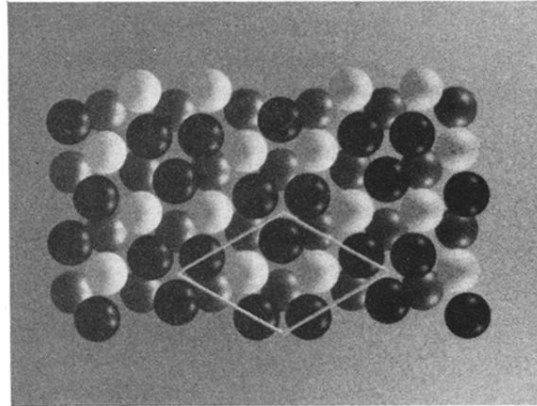
We have examined two models, one recently proposed on the basis of x-ray scattering results, the other first proposed in this paper, and find that both models are compatible with MEIS results. Both models have some disadvantages, but serve to illustrate the type of structure that must be postulated to exist on this surface. Further work on this system might involve determining whether either of these models are compatible with results of other experimental techniques or with theory. Construction of new models that overcome the difficulties discussed in this paper would also be a welcome development.

ACKNOWLEDGMENTS

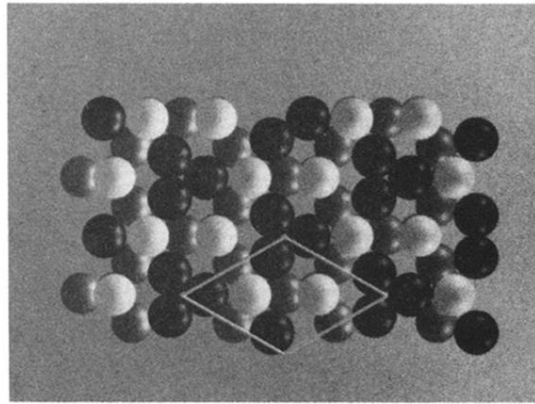
We would like to thank Mark Reuter for his assistance in obtaining the experimental results. We also wish to thank C. T. Chan, E. Vlieg, and E. J. van Loenen for sharing preliminary results with us.

-
- ¹E. J. van Loenen, J. E. Demuth, R. M. Tromp, and R. J. Hamers, *Phys. Rev. Lett.* **58**, 373 (1987).
²R. J. Wilson and S. Chiang, *Phys. Rev. Lett.* **58**, 369 (1987).
³R. J. Wilson and S. Chiang, *Phys. Rev. Lett.* **59**, 2329 (1987).
⁴M. Saitoh, F. Shoji, K. Oura, and T. Hanawa, *Surf. Sci.* **112**, 306 (1981).
⁵Y. Tereda, T. Yoshizuka, K. Oura, and T. Hanawa, *Surf. Sci.* **114**, 65 (1982).
⁶J. Stöhr, R. Jaeger, G. Rossi, T. Kendelewicz, and I. Lindau, *Surf. Sci.* **134**, 813 (1983).
⁷Y. Horio and A. Ichimiya, *Surf. Sci.* **164**, 589 (1985).
⁸S. Kono, K. Higashiyama, and T. Sagawa, *Surf. Sci.* **165**, 21 (1986).
⁹M. Aono, R. Souda, C. Oshima, and Y. Ishizawa, *Surf. Sci.* **168**, 713 (1986).
¹⁰S. Kono *et al.*, *Phys. Rev. Lett.* **58**, 1555 (1987).
¹¹R. M. Tromp and E. J. Van Loenen, *Surf. Sci.* **155**, 441 (1985).
¹²J. M. Nicholls, F. Salvan, and B. Reihl, *Phys. Rev. B* **34**, 2945

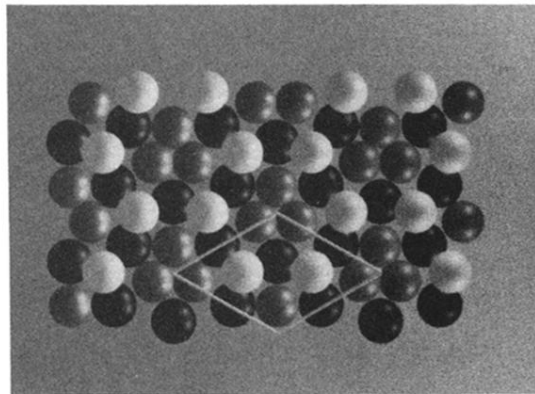
- (1986).
¹³T. Yokotsuka, S. Kono, S. Suzuki, and T. Sagawa, *Surf. Sci.* **127**, 35 (1983).
¹⁴J. F. van der Veen, *Surf. Sci. Rep.* **5**, 199 (1985).
¹⁵M. Copel and R. M. Tromp, *Phys. Rev. B* **37**, 2766 (1988).
¹⁶M. Copel, R. M. Tromp, and U. K. Köhler, *Phys. Rev. B* **37**, 10756 (1988).
¹⁷K. Takayanagi, Y. Tanishiro, M. Takahashi, and S. Takahashi, *J. Vac. Sci. Technol. A* **3**, 1502 (1985).
¹⁸C. T. Chan and K.-M. Ho (unpublished).
¹⁹T. L. Porter, C. S. Chang, and I. S. T. Tsong, *Phys. Rev. Lett.* **60**, 1739 (1988).
²⁰E. Vlieg, A. W. van der Gon, J. F. van der Veen, J. E. Macdonald, and C. Norris, *Surf. Sci.* **209**, 100 (1989).
²¹P. M. J. Marée, K. Nakagawa, J. F. van der Veen, and R. M. Tromp, *Phys. Rev. B* **38**, 1585 (1988).
²²T. Takahashi, S. Nakatani, N. Okamoto, T. Ishikawa, and S. Kikuta, *Jpn. J. Appl. Phys. Pt. 2* **27**, L753 (1988).



(a) Embedded Trimer Model



(b) Silicon Adatom-Vacancy Model



(c) Silver Honeycomb-Chained Trimer Model

FIG. 4. Models of the $\text{Si}(111)-(\sqrt{3} \times \sqrt{3})R30^\circ \text{Ag}$ surface. Top views include (a) the embedded trimer model, (b) the silicon adatom-vacancy model, and (c) the silver honeycomb-chained trimer model. Silver atoms are represented by the larger diameter spheres, and a $\sqrt{3} \times \sqrt{3}$ unit cell is indicated.